Electrochemical growth of iron and cobalt arborescences under a magnetic field: A TEM study

S. Bodea,[1,*] R. Ballou,[1,†] L. Pontonnier,[2,‡] and P. Molho[1,§]
[1]*Laboratoire Louis Néel, CNRS, Boite Postale 166, 38042 Grenoble Cedex 9, France*
[2]*Laboratoire de Cristallographie, CNRS, Boite Postale 166, 38042 Grenoble Cedex 9, France*
(Received 28 May 2002; revised manuscript received 26 August 2002; published 10 December 2002)

TEM observations of iron and cobalt arborescences grown by electrodeposition were performed. In the limited range of external parameters allowing the growth of such arborescences, the morphology at the nanometric scale is dendritic, and single crystalline dendrites are observed as long as 2 μm. The crystallographic structure of the dendrites is examined in detail. A magnetic field was applied during the growth, either parallel or normal to the plane of growth. Its effects on the morphology at the nanometric scale and on the crystallographic structure are analyzed.

DOI: 10.1103/PhysRevB.66.224104 PACS number(s): 61.43.Hv, 68.37.Lp, 81.15.Pq, 75.90.+w

I. INTRODUCTION

A wide range of physical, chemical and biological systems give rise to arborescent patterns, often through a far from equilibrium growth process.[1,2] One of the most challenging problems is to understand the origin of these patterns, to predict their formation from basic mechanisms, and to look for possible universalities. ''Simple'' systems, easier to investigate experimentally and theoretically, such as the solidification from an undercooled melt,[3,4] the viscous fingering,[5] the electrochemical deposition,[6,7] or more recently the formation of bacterial colonies[8,9] are therefore actively studied and a lot of efforts are made to find analogies between them.[1–5,8–10]

The electrochemical deposition of metals in thin gap geometry is one of the experimental systems allowing the formation of ramified patterns. Different macroscopic morphologies, empirically named dendritic, dense-radial, stringy, needlelike, open, etc.,[11,12] can be obtained as a function of several external parameters: applied voltage, initial concentration, etc. The rich variety of these morphologies results from the interplay of the different processes involved, which can be chemical and associated with the process of metal reduction, or physical and concerned with the dynamics of ions in a solution and under an electric field, i.e., diffusion, migration, or transport through fluid convections.

Since the first experiment of Matsushita *et al.*,[6] who obtained quasi-two-dimensional zinc fractal aggregates by electrochemical deposition, the primary intent of many studies of such metallic arborescences was to establish the dependency of macroscopic morphologies on the experimental parameters controlling the growth. Different ''phase'' diagrams as a function of the initial concentration and the applied voltage were thus reported.[11,12] To get further insights requires the investigation of the morphology and the structure of the arborescences at a nanometric scale, in order to understand the relationship between the mechanisms of the growth at that scale and the resulting macroscopic morphology. Unfortunately, such a characterization is rather difficult since the aggregates cannot be removed from the solution without being destroyed and they have a short lifetime in the solution after growth, most often becoming oxidized. For this reason, even the usually commodious scanning electron microscopy (SEM) was so far used only in the case of so-called ''robust deposits,'' i.e., ramified aggregates grown on a substrate,[13,14] in an agitated solution,[15,16] or in a paper support,[17,18] when the recovery of the aggregates after growth is possible.

The first characterization at a nanometric scale of arborescent aggregates obtained in a classical thin electrochemical cell, floating in the solution, was made by Grier *et al.*[12] by transmission electron microscopy (TEM). They showed that in the case of zinc, the dendritic morphologies were characterized by a crystalline order at a nanometric scale. Those dubbed DLA-like, because of the strong analogy with the pattern generated by the numerical model of diffusion-limited aggregation,[19] showed no crystalline order at that scale. This was confirmed in a following paper[20] where a model was proposed to explain the formation of crystalline dendrites very far from equilibrium. To our knowledge, since this last study no other characterization by TEM of such aggregates was made.

We report in this paper a TEM study of iron and cobalt arborescences grown by electrochemical deposition in a thin cell. We present a characterization of the morphology and the crystalline structure of the arborescences at the nanometric scale and the magnetic field effects on the growth at that scale to be related to the effects observed at a macroscopic scale, presented elsewhere.[21,22]

II. EXPERIMENTAL DETAILS

The experimental setup was described in detail in a previous paper.[21] In short, the experiments are performed in a circular geometry and at constant applied voltage. We used simple aqueous $Fe(SO_4)$ and $Co(SO_4)$ solutions, without a supporting electrolyte. The anode is a copper ring of diameter 4 cm and thickness 0.5 mm and the cathode is a copper wire of thickness 0.05 mm. A thin film of the solution ($\approx$500 μm thick) is spread on a glass plate, edged by the anode. Unlike previous similar experiments,[11,12] the cell is left open to reduce the destructive effect on the deposit of the H_2 bubbles generated during growth. A magnetic field up to 0.2 T, perpendicular or parallel to the cell plane, may be applied during the growth, using a ''magnetic mangle,'' a system built with permanent magnets (see Ref. 21).

For the TEM study we used a CM300 Philips microscope

equipped with an x-ray microanalysis system by energy dispersion (EDX). The energy of the electrons is 300 KeV, leading to a wavelength of about 0.0196 Å. Electron diffraction patterns are obtained in selected area.

The deposits are floating in the solution and very fragile and removing them from the solution after the growth destroys the very small branches. Usually, to perform measurements after the growth is completed, the deposit is left to dry on a glass coverslip put into the solution under the cathode. Unfortunately this leads to a degradation of the aggregates that are oxidized and polluted by residual salt from the solution. Therefore for the TEM study the samples are prepared following a different method. Instead of leaving the sample to dry, we use a grid of gold, which is part of the sample holder for the TEM observations, to recover parts of the aggregate still floating in the solution. This grid, of diameter 3 mm and thickness 0.1 mm, is a 100 μm$\times$100 μm square mesh, made of gold wire of thickness 20 μm, covered with an amorphous carbon membrane with holes. To recover the sample, the grid is simply dipped into the solution, under the aggregate, then lifted. The macroscopic morphology of the arborescence is lost, but the very small branches are preserved intact. Scanning the grid, we are able to find small dendrites in a good position to be analyzed, on the edge of the holes of the grid. This method limits the oxidation and the degradation of the arborescences that occurs during drying in the solution.

Due to the size of the analyzed domain and also to the limitation of the thickness that can be examined by TEM, one single observation may not be representative of the whole sample. Therefore acceptable statistics were realized, by examining different places on the same sample and also different samples coming from the same aggregate.

III. GROWTH WITHOUT MAGNETIC FIELD

The macroscopic morphologies are described in detail in Ref. 22 and, concerning iron arborescences, partly in Ref. 21. In short, because of H_2 formation during growth, iron and cobalt arborescences are obtained in a narrow range of external parameters: initial concentration $\mathcal{C}$ between 0.03 M and 0.5 M , applied voltage $\mathcal{U}$ between 3 V and 7 V for iron, $\mathcal{C}$ between 0.1 M and 0.5 M, $\mathcal{U}$ between 3 V and 8 V for cobalt. Concerning iron, only two different morphologies are found. A ''dense morphology,'' isotropic, with a very stable circular envelope, similar to that dubbed ''dense branching morphology'' (DBM) in the literature, is obtained for C between 0.03 M and 0.1 M. An example is displayed in Fig. 1(a). Optical microscopy performed during the growth gives more details, showing that the growth appears dendritic [Fig. 1(b)]. A well-defined angle is observed between the main and the secondary branches, but this angle is only local and the dendritic branches loose their orientation at larger scale. For higher concentration a ''sparse morphology'' is obtained, with only few branches, thicker and more ramified [Fig. 1(c)]. Concerning cobalt, only the sparse morphology could be obtained in the mentioned concentration range and constant applied voltage. The dense morphology was obtained

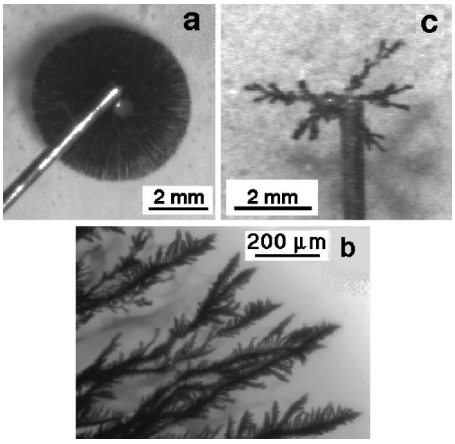

FIG. 1. Dense arborescence (iron, initial concentration $\mathcal{C}=0.06M$, applied voltage $\mathcal{U}=5$ V): (a) macroscopic view, (b) microscopic view. (c) Sparse arborescence (iron, $\mathcal{C}=0.5M$, $\mathcal{U}=5$ V): macroscopic view

''monitoring'' the applied voltage by limiting the current, but is not considered here.

Iron and cobalt arborescences were examined by TEM. We present here the results, first in the case of iron and then in the case of cobalt.

A. Iron arborescences

In the case of iron, samples from aggregates showing the two different macroscopic morphologies were considered. Two examples are shown in Fig. 2, one from a dense and one from a sparse arborescence. In both cases the branches appear dendritic at the TEM level. In fact the morphologies of the two branches are very similar and they could have been both observed in a dense arborescence. Consequently, nothing at the TEM scale allows one to distinguish between the macroscopically sparse and dense morphology. One difference, however, exists within the statistics of our observations: thin branches are more difficult to find in sparse than in dense aggregates, which could mean that the branches of sparse arborescences are thicker or that they contain less thin branches.

As a second step for the characterization of the arborescences, selected area electron diffraction was performed on

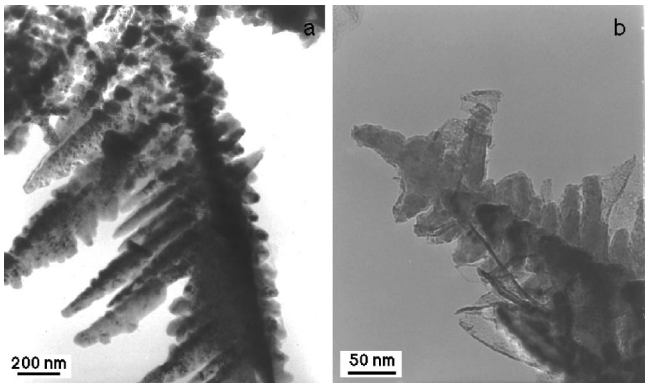

FIG. 2. TEM observations of iron arborescences grown without magnetic field: (a) dense morphology ($\mathcal{C}=0.06M$, $\mathcal{U}=5$ V), (b) sparse morphology ($\mathcal{C}=0.5M$, $\mathcal{U}=5$ V).

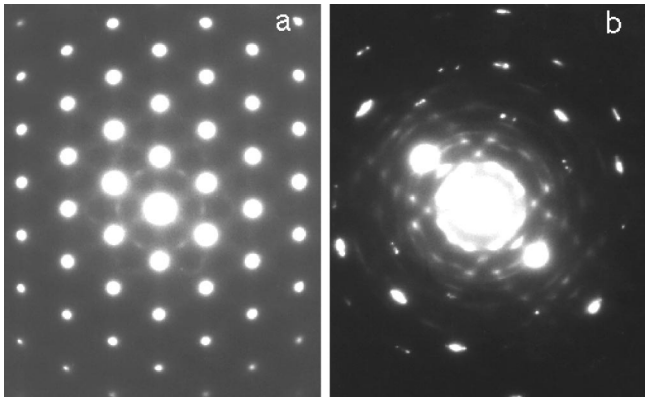

FIG. 3. Diffraction patterns of iron arborescences grown without magnetic field, corresponding to bcc phase: (a) the most commonly observed, zone axis [111]; (b) zone axis $[1\bar{1}0]$.

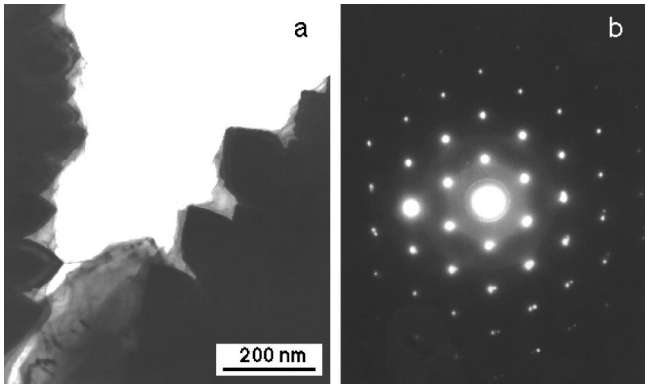

FIG. 4. (a) TEM image of a dendritic branch from a cobalt arborescence grown without magnetic field ($\mathcal{C}=0.5M$, $\mathcal{U}=5$ V); (b) corresponding diffraction pattern (zone axis [001] of the hcp structure).

the observed dendritic branches. The resulting diffraction patterns show that the branches of the arborescences are single crystalline at this level. Although consistent with the fact that the branches appear dendritic at this scale, this finding is rather surprising with regard to the observed macroscopic morphology. Indeed the DBM morphology is generally associated with tip-splitting processes, leading to non crystalline structure.[23] Accordingly the dense morphology is not rigorously what is actually considered as DBM.

We found no difference between the crystallization of the branches from dense or from sparse aggregates. The most typical diffraction pattern found in our study is shown in Fig. 3(a). The diffracted spots are related to the bcc structure of iron, with [111] as the zone axis. A less frequent diffraction pattern, with $[1\bar{1}0]$ as the zone axis, is shown in Fig. 3(b). The main spots show asymmetric shapes indicating that strong local crystal distortions exist in the bcc phase. In both diffraction patterns additional reflections can be observed. In the first diagram [Fig. 3(a)], where the main spots are oversaturated, some diffuse intensity, not related to the bcc phase, can be observed. In the second one [Fig. 3(b)] less intense diffraction peaks are present, arranged in a periodic way, indicating a superstructure. These supplementary diffraction peaks do not belong to the bcc phase of iron. Their position and their orientation with respect to the bcc main phase lead us to interpret the diffraction patterns in terms of ordered microdomains of some other phase, nucleated into the bcc iron phase.

To find out the nature of these microdomains we first considered the possibility that they belong to the iron oxide Fe_3O_4, the nucleation of micro domains of this oxide into a bcc iron phase having already been observed.[24] However, in our case, it is not possible to interpret all the observed diffraction patterns on the basis of this hypothesis.

We considered then the possibility that the observed diffraction patterns result from the nucleation of microdomains of fcc iron into the bcc iron phase. The weak diffuse intensity observed in Fig. 3(a) can be associated with such a nucleation. The superstructure diffraction peaks in Fig. 3(b) can be interpreted as satellites around the fcc peaks. These satellites are arranged in a crosslike shape, the two branches of the cross being in the $\langle 110\rangle$ direction of fcc Fe or in the $\langle 100\rangle$ direction of bcc Fe. This is in good agreement with the geometrical relations between the two types of structure. The satellites around the fcc peaks are defining a larger periodicity than the fcc lattice. These ordered microdomains of the fcc phase induce distortions in the bcc phase, resulting in deformations of the spots of the bcc main phase. Similar superstructure reflections are found in the case of microdomains with antiphase boundaries.[25]

In many diagrams two diffraction rings are also observed. After a careful analysis of the diffraction pattern and some complementary x-ray microanalysis we attributed the first one to the iron oxide Fe_3O_4 and the second one to the anhydrous iron sulfate $Fe(SO_4)$. These two compounds are finely divided at the surface of the arborescences and present only in a very small quantity, as deduced from the small intensity of the diffraction rings.

All the diffraction patterns show that the observed dendritic branches are single crystalline. Therefore their growth direction has to coincide with a crystallographic axis. To determine this direction, the angle between the main and the secondary branches was measured and found to be close to 60°. Assuming that the dendrites lay horizontally on the grid, a 60° angle suggests that they are growing along the $\langle 110\rangle$ directions with the $\langle 111\rangle$ direction perpendicular to the plane of growth. Indeed, we found some diffraction patterns with $\langle 110\rangle$ in the plane of growth and $\langle 111\rangle$ perpendicular to this plane. However, other growth directions could not be excluded and in this case, the angle close to 60° may be explained by the fact that the dendrites are not horizontal on the grid.

B. Cobalt arborescences

In the case of cobalt we considered only samples from aggregates showing a sparse macroscopic morphology. The end of a branch is shown in Fig. 4(a), and the corresponding diffraction pattern in Fig. 4(b). Similar to iron, the branches are dendritic and single crystalline at the TEM level. The diffraction peaks observed in Fig. 4(b) correspond to the hexagonal compact (hcp) phase of cobalt. The diffraction plane

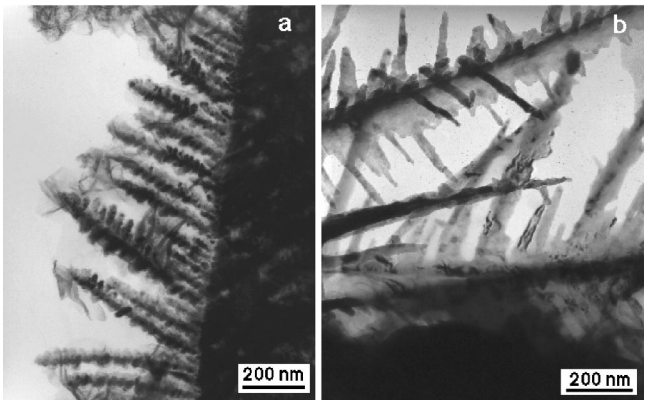

FIG. 5. TEM images of iron dendrites grown under an in-plane magnetic field: (a) dense morphology ($\mathcal{C}=0.06M$, $\mathcal{U}=5$ V), (b) sparse morphology ($\mathcal{C}=0.5M$, $\mathcal{U}=5$ V).

contains the [100] and [010] axis and the [001] axis is perpendicular to the plane. As for iron, two continuous rings are observed on the diffraction patterns, one corresponding to Co_3O_4 and the other to $Co(SO_4)$. Again, these two compounds are present in very small quantities and finely divided at the surface of the arborescences.

IV. GROWTH UNDER AN IN-PLANE MAGNETIC FIELD

The effects at the macroscopic scale of a magnetic field applied in the plane of growth are detailed in Ref. 21 for iron arborescences and in Ref. 22 for both iron and cobalt arborescences. In short when an in-plane field of 0.2 T is applied during the growth of iron and cobalt arborescences, the macroscopic morphology changes. ''Sparse'' morphology becomes elongated in the direction of the field, with two thick branches parallel to the field. ''Dense'' morphology is also affected, in a spectacular way: the isotropic circular shape of the arborescence becomes rectangular. Optical microscopy revealed that this shape results from a selection of the orientation of the growing branches with respect to the applied magnetic field.

We performed TEM observations to study these effects at a nanometric scale. Samples from iron and cobalt arborescences grown under in-plane magnetic field were considered.

A. Iron arborescences

In the case of iron, a large number of observations were performed on samples with a dense macroscopic morphology and only a few observations on one single sample showing a sparse macroscopic morphology. Two examples of branches, one coming from a dense aggregate and the other from the sparse one, are shown in Fig. 5. No specific magnetic field effect on the morphology is observed at this scale on the dense arborescences. Concerning sparse arborescences, it seems that some magnetic field effects on the growth exist: the branches are more needlelike than in the case of growth without applied magnetic field. However, only a few observations were performed and more detailed experiments are needed to be conclusive. Concerning the structure of the branches, no signature of the magnetic field at the TEM level

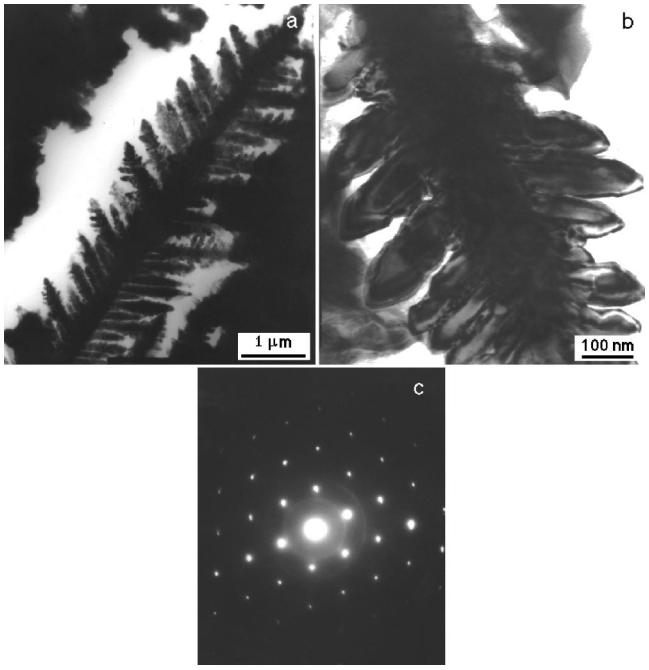

FIG. 6. (a, b) TEM images of dendritic branches from a cobalt arborescence grown under an in-plane magnetic field ($\mathcal{C}=0.5M$, $\mathcal{U}=5$ V); (c) corresponding diffraction pattern, showing distortions of the diffraction plane (zone axis [001] of the hcp structure).

was observed. We found the same diffraction patterns for branches coming from sparse or dense arborescences, obtained with or without in-plane magnetic field. One should point out, however, that the local character of the TEM observations does not allow information about the absolute orientation of the branches with respect to the applied magnetic field.

B. Cobalt arborescences

In the case of cobalt, we performed observations only on samples from sparse arborescences, as when no magnetic field was applied. Two examples of branches, at different scales, are shown in Fig. 6. Here again the branches are dendritic and no specific magnetic field effect appears at this scale. The same plane is observed on the diffraction pattern [Fig. 6(c)], with the [001] zone axis of the hcp structure always perpendicular to the plane. However, one can see distortions of the diffraction plane and that the intensities of equivalent peaks are not equal. These kinds of distortions are often observed in the case of cobalt, generally related to stacking faults.

V. GROWTH UNDER A NORMAL MAGNETIC FIELD

The effects at the macroscopic scale of a magnetic field applied perpendicular to the plane of growth are detailed in Ref. 22 for both iron and cobalt arborescences. When a normal magnetic field is applied during the growth, a spiraling macroscopic morphology is observed in the case of nonmagnetic arborescences. The spiraling morphology is understood as resulting from a convective motion of the solution induced

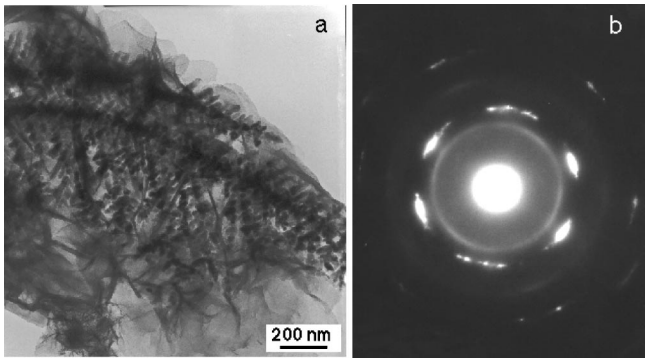

FIG. 7. (a) TEM image of a dendritic branch from an iron arborescence grown under a magnetic field perpendicular to the plane of growth ($\mathcal{C}=0.06M$, $\mathcal{U}=5$ V); (b) corresponding diffraction pattern. The observed ring can be attributed to finely divided Fe_3O_4 at the arborescence surface (see text).

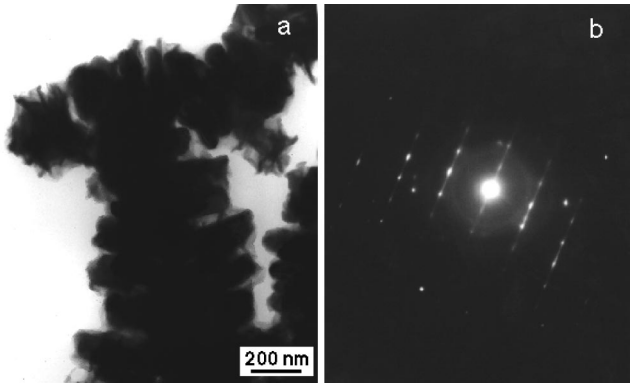

FIG. 8. (a) TEM image of a dendritic branch from a cobalt arborescence grown under a magnetic field perpendicular to the plane of growth ($\mathcal{C}=0.5M$, $\mathcal{U}=5$ V); (b) corresponding diffraction pattern.

by the Lorentz force acting on every charged particle moving in the magnetic field. This effect is known in the literature as the magnetohydrodynamic effect (MHD).[26]

In the case of iron and cobalt arborescences, a normal magnetic field applied during the growth induces no spiraling. A change in the morphology is observed: sparse arborescences become more ramified with thicker branches, dense arborescences become thinner and less ramified. The convective motion of the solution still exists, which means that the inhibition of the spiraling morphology has to be related to the magnetic character of the aggregates, probably through the dipolar interactions between magnetized branches. TEM observations were performed on samples from dense aggregates for iron and from sparse aggregates for cobalt.

A. Iron arborescences

An example of a dendritic branch from an iron dense aggregate is shown in Fig. 7(a). The applied magnetic field was about 0.2 T. One can observe that the branch is bent, reminiscent of the spiraling observed at the macroscopic scale in the case of nonmagnetic aggregates. A typical diffraction pattern of such a curved branch is shown in Fig. 7(b). The branch is single crystalline and the diffraction peaks correspond to the 110 reflections of the bcc iron. The zone axis is [111]. The diffraction peaks are arched, indicating that strong distortions exist in the crystal. The presence of these arched spots can be associated with a progressive rotation of the dendrite axis $[1\bar{1}0]$ or, equivalently, with a progressive rotation of the crystal around the zone axis.[27] The observation of curved dendritic branches, related to the presence of arched spots in the diffraction patterns, shows that the spiraling morphology seems to be present at the TEM level. This leads to the conclusion that the inhibition of the spiraling morphology is taking place at an intermediate level, between the macroscopic level where no spiraling is observed and the TEM level where the spiraling morphology seems to be present.

B. Cobalt arborescences

The experiments were more difficult to perform in the case of cobalt. It seems that the branches are thicker and only a few branches were thin enough to be examined by TEM. One of the observed branches is presented in Fig. 8(a). It comes from a cobalt aggregate grown under a normal magnetic field of about 0.2 T. This branch is different from the other dendritic branches that we observed previously and no curvature of the main branch appears. The corresponding diffraction pattern is shown in Fig. 8(b). The branch is single crystalline in this case again and the most intense diffraction peaks correspond to the hcp cobalt phase. However, in contrast with the growth performed in zero or in-plane magnetic field, here the [001] axis (i.e., the $\vec{c}$ axis of the hcp structure) is within the plane of growth. The other axis within this plane is [100], perpendicular to the $\vec{c}$ axis. It is not possible to identify the growth axis in the TEM image [Fig. 8(a)] since the dendrite is too thick, but the square shape observed in this image is consistent with the growth axis of the dendrite being the $\vec{c}$ axis of the hcp structure. An additional diffuse intensity is also observed in the diffraction pattern, organized in lines parallel to the $\vec{c}^*$ direction. This is usually observed in the case of hcp structures and indicates the presence of stacking faults in the crystal. These faults correspond to the fcc cobalt phase and such a diffraction pattern can be understood as resulting from fcc domains of different sizes present into the hcp main phase. This effect of the magnetic field, which is to flip the $\vec{c}$ axis of the hexagonal structure from perpendicular to a direction in the plane of growth, is similar to what is observed in nanowires of cobalt grown by electrodeposition in a nanoporous membrane.[28] In such nanowires, depending on the value of the overpotential applied to initiate the growth, the $\vec{c}$ axis may be perpendicular or along the geometrical axis of the wire. In the latter case, distortions of the hcp structure appear clearly as stackings of hcp and fcc phases. The diffraction patterns observed in both cases are very similar to those observed in cobalt arborescences.

VI. CONCLUSION

To summarize, this TEM study shows a strong analogy between iron and cobalt arborescences. In both cases, the

branches of aggregates grown in zero magnetic field are single crystalline dendrites on the nanometric scale. In the case of iron, growth takes place probably in the plane perpendicular to the [111] axis of the bcc structure and, in the case of cobalt, in the plane perpendicular to the $\vec{c}$ axis of the hcp structure. Nucleation of microdomains into the main phase is also observed in both cases: domains of the fcc phase into the bcc phase for iron and domains of the fcc phase into the hcp phase for cobalt.

Concerning the growth under in-plane magnetic field, no signature of the applied field is observed at the TEM level for both iron and cobalt, while on a macroscopic scale the magnetic field induces strong effects via the dipolar interactions between magnetized branches.

Concerning growth under a normal magnetic field, the effect at the TEM scale is, for iron, a distortion of the cubic cell and, for cobalt, a flip of the axis of the hexagonal cell from perpendicular to parallel to the plane of growth. At a macroscopic scale, on the other hand, the typical spiraling morphology obtained for nonmagnetic arborescences is not observed. Some questions about these normal magnetic field effects are still open: to what extent are the two different effects, the distortion of the cubic cell (iron) and the flip of the axis of the hexagonal structure (cobalt) related, since they are a crystallographic response to the same constraint, the normal magnetic field? How are these effects related to the Lorentz force acting on the ions moving in the solution? TEM observations of nonmagnetic arborescences of different crystalline structures, grown under normal magnetic field, should be of interest to answer these questions.

Magnetic field effects on the growth of magnetic arborescences, observed at a macroscopic scale, are interpreted as resulting from dipolar interactions between the growing branches, magnetized in the applied field. Since those effects are not seen at the TEM scale (no effect of in-plane field and no inhibition of the effects of the rotating fluid induced by Lorentz forces in normal magnetic field), the conclusion is that dipolar effects are taking place at an intermediate scale, larger than the one observed by TEM. Experiments at that intermediate scale, for instance, microdiffraction with synchrotron radiation, are necessary to understand precisely through which mechanism dipolar interactions lead to the observed macroscopic effects.

*Present address: Max Planck Institut für Mikrostruktur Physik, Weinberg 2, D-06120 Halle, Germany. Electronic address: sbodea@mpi-halle.mpg.de

†Electronic address: ballou@grenoble.cnrs.fr

‡Electronic address: liliane.pontonnier@grenoble.cnrs.fr

§Electronic address: molho@grenoble.cnrs.fr

[1] *Branching in Nature*, edited by V. Fleury, J.-F. Gouyet, and M. Leonetti (Springer-Verlag, Berlin, and EDP Sciences, Les Ulis, 2001).

[2] M.C. Cross and P.C. Hohenberg, Rev. Mod. Phys. **65**, 851 (1993).

[3] M. E. Glicksman and S. P. Marsh, in *Handbook of Crystal Growth*, edited by D. T. J. Hurle (North-Holland, Amsterdam, 1993), 1b, p. 1075, and references therein.

[4] J.S. Langer, Rev. Mod. Phys. **52**, 1 (1980) and references therein.

[5] *Dynamics of Curved Fronts*, edited by P. Pelcé (Academic, New York, 1988), and references therein.

[6] M. Matsushita, M. Sano, Y. Hayakawa, H. Honjo, and Y. Sawada, Phys. Rev. Lett. **53**, 286 (1984).

[7] R.C. Brady and R.M. Ball, Nature (London) **309**, 225 (1984).

[8] E. Ben-Jacob, I. Cohen, and H. Levine, Adv. Phys. **49**, 395 (2000) and references therein.

[9] *Fluctuations and Scaling in Biology*, edited by T. Vicsek (Oxford University Press, New York, 2001) and references therein.

[10] D.A. Kessler, J. Koplik, and H. Levine, Adv. Phys. **37**, 255 (1988).

[11] Y. Sawada, A. Dougherty, and J.P. Gollub, Phys. Rev. Lett. **56**, 1260 (1986).

[12] D. Grier, E. Ben-Jacob, R. Clarke, and L.M. Sander, Phys. Rev. Lett. **56**, 1264 (1986).

[13] V. Fleury and D. Barkey, Europhys. Lett. **36**, 253 (1996).

[14] V. Fleury and D. Barkey, Physica A **233**, 730 (1996).

[15] A.R. Imre, Z. Vertesy, T. Pajkossy, and L. Nyikos, Fractals **1**, 59 (1993).

[16] A.R. Imre and L. Balazs, Fractals **8**, 349 (2000).

[17] D.B. Hibbert and J.R. Melrose, Phys. Rev. A **38**, 1036 (1988).

[18] D.B. Hibbert and J.R. Melrose, Proc. R. Soc. London, Ser. A **423**, 149 (1989).

[19] T.A. Witten and L.M. Sander, Phys. Rev. Lett. **47**, 1400 (1981).

[20] D.G. Grier, K. Allen, R.S. Goldman, L.M. Sander, and R. Clarke, Phys. Rev. Lett. **64**, 2152 (1990).

[21] S. Bodea, L. Vignon, R. Ballou, and P. Molho, Phys. Rev. Lett. **83**, 2612 (1999).

[22] S. Bodea, R. Ballou, and P. Molho (unpublished).

[23] D.G. Grier, D.A. Kessler, and L.M. Sander, Phys. Rev. Lett. **59**, 2315 (1987).

[24] M. Cahoreau and M. Gillet, J. Microsc. (Paris) **4**, 207 (1965).

[25] H. Sato and R.S. Toth, Phys. Rev. **124**, 1833 (1961); H. Sato and R.S. Toth, *ibid.* **127**, 469 (1962).

[26] T.Z. Fahidy, J. Appl. Electrochem. **13**, 553 (1983).

[27] S. Amelincks, A. Lucas, and P. Lambin, Rep. Prog. Phys. **62**, 1471 (1999).

[28] G. Tourillon, L. Pontonnier, J.-P. Levy, and V. Langlais, Electrochem. Solid-State Lett. **3-1**, 20 (2000).